JOURNAL OF CATALYSIS 116, 361–372 (1989)

Characterization of Zn-Promoted Rh/SiO_2 Catalysts by Chemisorption, Infrared Spectroscopy, and Temperature-Programmed Desorption

H. W. JEN, Y. ZHENG, D. F. SHRIVER, AND W. M. H. SACHTLER

Catalysis Center and Department of Chemistry, Northwestern University, Evanston, Illinois 60208

Received July 6, 1988; revised November 16, 1988

Rh/SiO_2 samples with various atomic ratios of Zn to Rh were prepared by impregnation of the chlorides, followed by reduction in hydrogen. X-ray photoelectron spectra indicate that for low Zn/Rh ratios, the Zn ions are preferentially located on the surface of the Rh particles, whereas the Cl ions are efficiently removed. For high Zn/Rh ratios, $ZnCl_2$ is deposited on the surface of the SiO_2 support. The chemisorption of CO and H_2 decreases with increasing Zn loading. Fourier transform infrared spectroscopy reveals that added Zn leads to a decrease in the proportion of bridging CO. Temperature-programmed desorption (TPD) shows that reactive desorption of CO to form methane is strongly depressed by Zn. These results are consistent with a model that assumes that Zn blocks the rhodium ensembles for CO dissociation and subsequent methane formation.

INTRODUCTION

The hydrogenation of carbon monoxide is catalyzed by numerous transition metals; the predominant product of this Fischer–Tropsch process is a mixture of hydrocarbons. Activity and selectivity of this process depend on the catalyzing metal, and they can be strongly altered by additives which we shall call "catalyst promoters," although they may also serve as supports (*1–5*). For Pd as the catalyzing metal such additives can direct the reaction toward methanol (*5–9*). For Rh catalysts that were prepared by decomposing $Rh_4(CO)_{12}$ on various metal oxides, Ichikawa found that marked changes in activity and selectivity were induced by the supporting oxide (*3, 4*). With ZnO, CaO, or MgO the selectivity to methanol exceeded 90%. The formation of higher alcohols, aldehydes, and organic acids was promoted by adding the chlorides of Mn, Ti, Zr, or Fe to Rh/SiO_2 (*4*). Promotion of C_2-oxygenates by addition of Mn to Rh/SiO_2 was reported earlier by Wilson *et al.* (*2*). The effects of promoters on Pd/SiO_2 and on the formation of oxygenates have been studied by various authors (*6–13*).

It is widely accepted that surface alkyl groups are formed by hydrogenation of surface carbon, resulting from the dissociation of CO, followed by chain growth (*11, 14–16*). Insertion of CH_2 into a metal–alkyl bond is the simplest model for this step. An alternative process leading to the formation of a new C–C bond is the migratory insertion of surface CO into a metal–alkyl bond. The resulting acyl group can then leave the surface either as an aldehyde by picking up one H atom or as a primary alcohol by addition of three H atoms. A promoter that directs the conversion toward higher oxygenates should thus facilitate CO insertion into a metal–alkyl bond (*15–19*). This reasoning creates a link between this group of reactions and hydroformylation, a reaction for which it is obvious that CO insertion is taking place. In previous work we studied the effect of one of the above promoters, viz., Zn, on the hydroformylation of ethylene over Rh/SiO_2 (*20*). It was found that addition of small amounts of Zn strongly

0021-9517/89 $3.00

increased the hydroformylation, the selectivity, and the absolute yield of propionaldehyde. The IR spectra showed characteristic changes implying that the Zn promoter interferes with the adsorption of carbon monoxide (*20*). From these preliminary results it had to be concluded that part of the promoting species is present on the surface of the Rh particles and blocks sites used otherwise for the adsorption of CO or hydrogen. The present paper reports more detailed FTIR spectroscopic investigations along with temperature-programmed desorption (TPD) data for hydrogen and carbon monoxide and reductive desorption of CO into flowing hydrogen.

The present work was designed to collect experimental data that might be used to decide between the proposed models for the promoter effect of an electropositive metal in rhodium-catalyzed CO hydrogenation and olefin hydroformylation. The models are described here:

1. The promoter stabilizes positive ions of the catalytic metal (*8*, *16*).
2. The promoter is adsorbed on the metal surface as in SMSI systems, and it interacts with the adsorbed reactants by (a) blockage of specific sites; (b) short-range chemical or electrostatic interaction with one or more adsorbed reactants [for example, oxygen of CO is known to react with Lewis acids and thereby undergo migratory insertion, producing surface acyl groups (*15–18*)]; and (c) long-range (through metal or through space) interactions.
3. The promoter stabilizes certain reaction intermediates, e.g., a formate ion (*10*).

Our previous results gave credence to the idea that the Mn promoter effect on Rh/SiO_2 arises from short-range interaction between adsorbed CO and coadsorbed Mn ions, which leads to C- and O-bonded CO (*15*). There is, however, no reason for generalizing this conclusion to other promoters such as Zn, which is the object of the present work.

EXPERIMENTAL

Catalysts were prepared by the impregnation method. Silica gel (SiO_2) of Davison Grade 62 (60–80 mesh; surface area 260–280 m^2/g) was added into a methanol solution containing known amounts of $RhCl_3 \cdot 3H_2O$ (Johnson Matthey Inc.) and $ZnCl_2$ (anhydrous, Alfa Products). The solvent was then removed by evaporation at 45–60°C. The loading of Rh was about 4 wt% for each sample. Variation of the mole ratio of Zn to Rh was achieved by changing the Zn content. Prior to use, the catalyst was reduced *in situ* with H_2 by the following heating procedure: room temperature to 200°C in 2 h, 200°C for 2 h, 200 to 400°C in 2 h, and 400°C for 6 h.

All gases were ultrahigh purity from Matheson, and these were further purified by passage through molecular sieve 4A and MnO/SiO_2 to remove water and oxygen. Carbon monoxide was first passed through an Al_2O_3 trap to remove metal carbonyl impurities.

Infrared spectra of CO adsorbed on a catalyst wafer were recorded on a Nicolet 60 SX single-beam FT-IR spectrometer. Details of the cell, which has provisions for *in situ* reduction and CO adsorption, have been described elsewhere (*17c*). Generally, a wafer 7 mm in diameter was pressed from a sample of 8 mg catalyst. After catalyst reduction, the cell was purged by ultrapure He, and a background spectrum was recorded. Carbon monoxide at 1 atm was then passed through the cell at 50 cm^3/min for 15 min, the cell was again purged with He, a second spectrum was obtained, and the spectrum was subtracted. Gas-phase CO was not detected after the typical 30-min He purge. IR data were collected for another hour over which time changes were negligible, indicating stability of the sample and lack of significant oxygen contamination of the cell.

After reduction, some wafers were transferred in air from the IR cell to an X-ray photoelectron spectrometer (ESCALAB

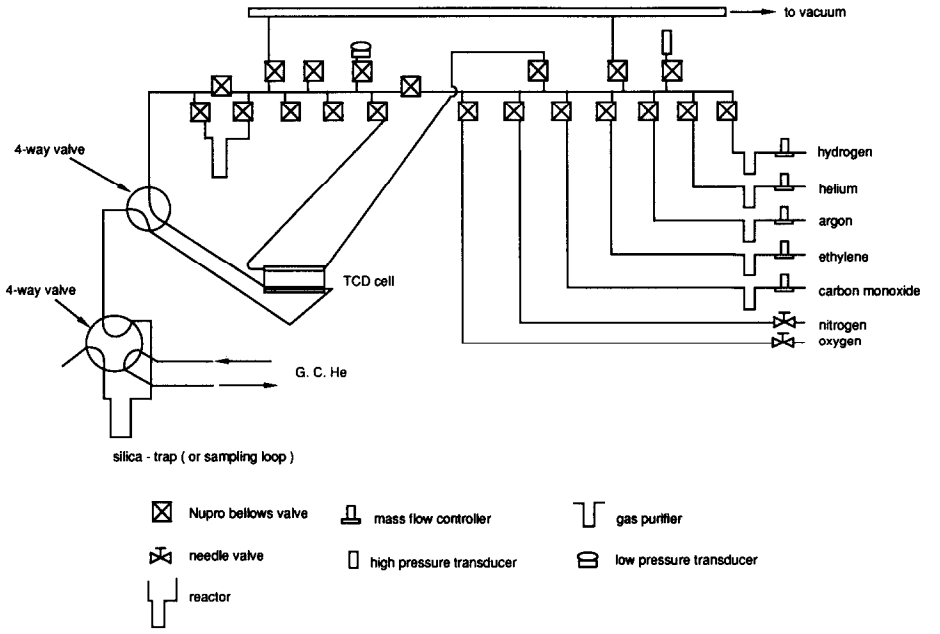

FIG. 1. Flow system for chemisorption, temperature-programmed desorption, and catalytic reaction.

MK II, VG Scientific). The wafers were degassed at 100°C without further reduction inside the spectrometer. The spectra were obtained to determine the relative ratios for Cl, Zn, and Rh on the catalyst surface.

A flow system made of stainless-steel tubing (Fig. 1) was used for chemisorption and TPD. The system can be evacuated to 10^{-6} Torr. A Pyrex glass reactor with a frit was used in this study. Chemisorption of H_2 or CO was measured volumetrically at room temperature. The following procedure was used in the chemisorption study: (1) a 0.2- to 0.5-g sample was reduced in the reactor, (2) the sample was evacuated at 400°C for 30 min and cooled to room temperature, (3) an adsorption isotherm was determined for CO or H_2, (4) the reactor was evacuated for 25 min, and (5) a second adsorption isotherm was determined. The first isotherm defines total adsorption and the second one, weak adsorption. The amount of strongly adsorbed CO or H is defined as the difference between the two adsorptions.

Chemisorption was always followed by TPD. The chemisorbed H was desorbed from 20 to 400°C into an Ar flow and CO from 20 to 500°C into a He or H_2 flow. The change in thermal conductivity due to gas desorption was measured with a thermal conductivity detector (TCD) cell and gas evolved was trapped on SiO_2 at −195°C. These gases were then analyzed on a gas chromatograph (HP 5870A) equipped with TCD and a carbosphere column (45 × 0.3 cm). Air, CO, CH_4, and CO_2 are separated and quantified. Differences in peak positions or integrated peak areas between samples of different Zn/Rh ratios are solely ascribed to different interactions between gas and surface, because the texture of the SiO_2 support and, consequently, all pore diffusion effects are identical.

RESULTS

Chemisorption

As indicated in Table 1, the addition of Zn to Rh/SiO_2 caused a decrease in adsorp-

TABLE 1

Adsorption of CO or H_2 on $RhZn/SiO_2$ at Room Temperature

Zn/Rh	Adsorption of CO (cm^3/g-cat)			Adsorption of H_2 (cm^3/g-cat)		
	Total	Weak	Strong	Total	Weak	Strong
0.00	2.10	0.34	1.76	1.27	0.48	0.79
0.05	2.13	0.30	1.83	1.22	0.45	0.77
0.075	2.01	0.28	1.73	1.25	0.34	0.91
0.11	1.70	0.32	1.38	1.07	0.44	0.63
0.30	0.92	0.21	0.71	0.50	0.31	0.19
1.10	0.91	0.27	0.64	0.51	0.32	0.19

TABLE 2

Effect of Zn on Chemisorption of H and CO over $RhZn/SiO_2$

Zn/Rh	CO/Rh	H/Rh	Dispersion from TEM
0.00	0.21	0.19	0.28
0.05	0.21	0.18	—
0.075	0.20	0.20	—
0.11	0.16	0.14	—
0.30	0.085	0.044	—
1.1	0.076	0.041	0.27

tion of both CO and H_2. The metal dispersion calculated from the amount of strongly adsorbed CO and H_2 is given in Table 2 for a number of Zn/Rh ratios. Transmission electron microscopy (TEM) (Table 2) shows that the size and morphology of the rhodium particles are virtually the same for the samples with Zn/Rh ratios equal to 0 and 1.1.

x-Ray Photoelectron Spectroscopy

The area ratios for the Cl (2*p*), Zn ($2p_{1/2}$), and Rh (3*d*) XPS peaks are presented in Table 3. No peaks of Cl or Zn were detected for unpromoted Rh/SiO_2. In the samples promoted with $ZnCl_2$ these elements were detectable. As the overall Zn/Rh ratio increased from 0.3 to 1.1, the area ratios of Cl/Zn and Cl/Rh increased substantially.

IR Spectroscopy

The FT-IR spectra are shown in Fig. 2 for strongly held CO which survived 100 min of He purge at room temperature. For Rh/SiO_2, two bands were observed. The band centered at 2054 cm^{-1} is attributed to linear (terminal) CO, whereas the low-frequency bands with peaks at 1912 and 1855 cm^{-1} are characteristic of C-bridging CO (*21–24*). During the He purge the positions of the IR bands for linear CO on $RhZn/SiO_2$ (Table 4) shifted about 10 cm^{-1} to higher frequency.

The addition of Zn lowers the intensity of the bridging CO band more than that of linear CO (Fig. 2A). For Zn/Rh 0.3 the bridging CO band disappeared (Fig. 2B). Meanwhile, a shoulder around 1960 cm^{-1} appeared along with the linear CO band. The area ratio of the bridging to linear CO bands decreased with increasing Zn/Rh from 0.0 to 0.11 (Table 4). No CO bands were observed for Zn/SiO_2.

For CO adsorbed on $RhZh/SiO_2$, a weak band was observed near 1597 cm^{-1} which appears to contain two components (Fig. 3). No corresponding band was detected for Rh/SiO_2 or Zn/SiO_2. The intensity of this band was about 1/50th that for the linear CO band. To assign bands in this region a study was made of adsorbed ^{13}CO. A dose of 15 cm^3 ^{13}CO onto freshly reduced $RhZn/SiO_2$ with Zn/Rh = 0.3 revealed three bands at 1620, 1553, and 1354 cm^{-1} (Fig. 3 curves a and b). The band at 1354 cm^{-1} corresponds

TABLE 3

Ratio of Surface Elements on Rhodium Samples from x-Ray Photoelectron Spectroscopy

Sample	Area ratio of XPS peaks[a]		
	Cl/Rh	Cl/Zn	Zn/Rh
$RhCl_3$–^3H_2O	0.53	—	0
Rh/SiO_2	0	—	0
$RhZn/SiO_2$ (Zn/Rh = 0.3)	0.038	0.075	0.50
$RhZn/SiO_2$ (Zn/Rh = 1.1)	0.12	0.18	0.68

[a] For Rh the area was integrated under both $3d_{3/2}$ and $3d_{5/2}$ peaks, which were merged in the spectra.

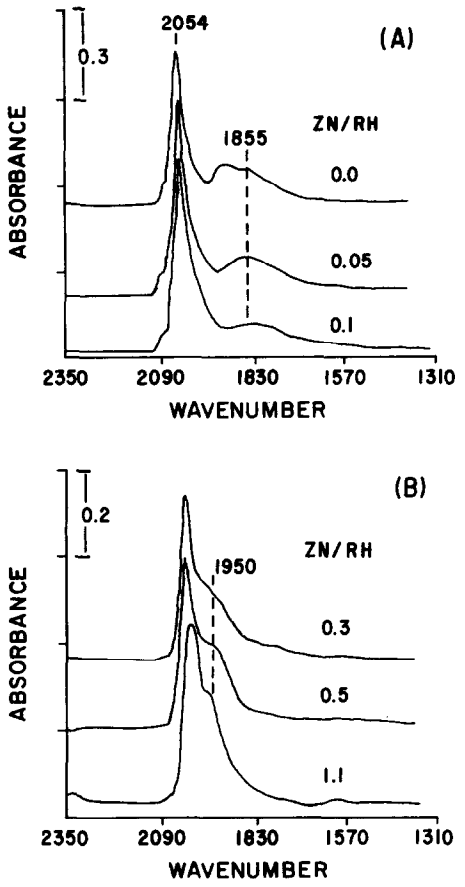

FIG. 2. IR spectra for adsorbed CO-on-$RhZn/SiO_2$ samples with various atomic ratios of Zn to Rh, after CO adsorption at room temperature and He purge for 100 min.

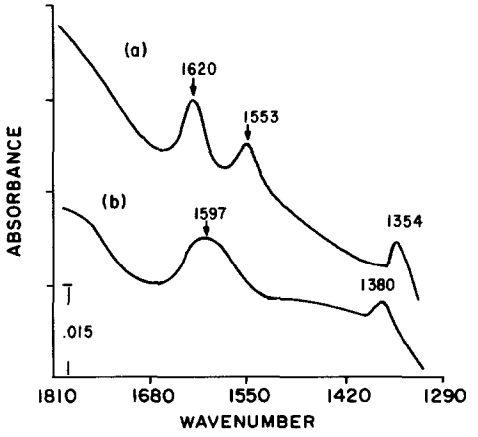

FIG. 3. IR spectra of adsorbed CO in the low-frequency range: (a) ^{13}CO, (b) ^{12}CO.

to a 1380 cm^{-1} band for ^{12}CO. Since its position is very close to the silica gel cutoff, it is subject to large uncertainty. Injection of CO_2 into a CO flow introduced new bands at 1413–1420 cm^{-1} for freshly reduced catalyst (Zn/Rh = 1.1). No significant changes were detected in the band at 1597 cm^{-1}.

TPD of Chemisorbed Hydrogen

As shown in Fig. 4, H_2 desorption from Rh/SiO_2 causes a broadband with a wide maximum from 125 to 200°C. This indicates multiple chemisorption sites for hydrogen. As the Zn/Rh ratio increases, the area of

TABLE 4

Result of IR Spectroscopy for Adsorbed CO over $RhZn/SiO_2$

	Zn/Rh ratio					
	0.0	0.05	0.11	0.30	0.50	1.1
t(min), He purge	20–170	20–185	20–130	20–170	20–110	25–145
Linear CO band (cm^{-1})	2067–2054	2054–2048	2052–2045	2039–2034	2039–2034	2032–2023
Bridged CO band (cm^{-1})	1912–1863	1856	1851	—	—	—
Range for linear CO	2080–1967	2080–1943	2080–1918			
Area for linear CO[a]	26.68	36.75	39.59	—	—	—
Range for bridged CO	1967–1612	1943–1612	1918–1612			
Area for bridged CO[a]	30.91	31.37	17.64	—	—	—
Ratio of bridged/linear	1.16	0.85	0.45			

[a] From the spectra in Fig. 2.

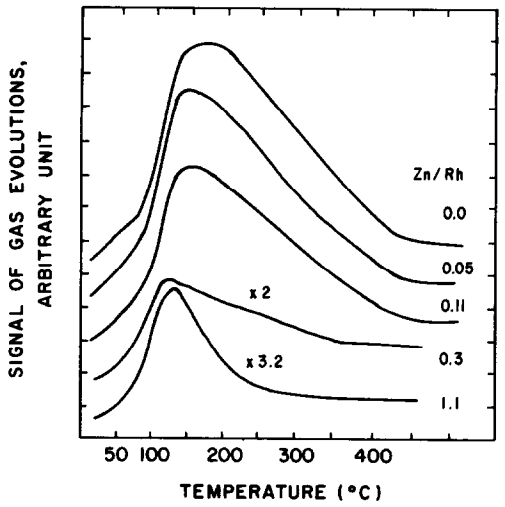

FIG. 4. Temperature-programmed desorption of hydrogen chemisorbed at room temperature: carrier gas = 25 cm³/min Ar, heating rate = 10°C/min. The ×2 and ×3.2 are the amplifying factors for the curves. (This is the same for the other figures.)

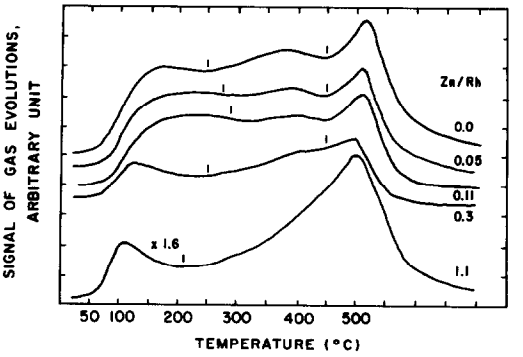

FIG. 5. Temperature-programmed desorption in helium of CO chemisorption at room temperature: carrier gas = 30 cm³/min helium, heating rate = 10°C/min.

the band decreases and it becomes sharper. The integrated TPD spectrum agrees with the chemisorption result.

TPD of Chemisorbed Carbon Monoxide

The number of accessible surface sites on the rhodium particles, Rh_s, is defined as the number of chemisorbed CO molecules. When desorbed into a H_2 or He flow with increasing temperature, CO, CO_2, and CH_4 were identified as released gases. The results in Fig. 5 and Table 5 have been corrected for the background due to residual methanol solvent.

The TPD spectra for chemisorbed CO in He are shown in Fig. 5. The tic marks above each spectrum indicate the temperatures at which the gases were analyzed. The identity and amount of desorbed gases are listed in Table 5. The TPD spectrum for Rh/SiO_2 showed multiple desorption peaks

TABLE 5

Gas Evolution during TPD of Chemisorbed CO in He

Zn/Rh	Total gas evolution[b] (per Rh_s)	Gas evolution in specified range[a] (per Rh_s)	Peak positions (°C)
0.0	0.830 CO + 0.165 CO_2 Σ = 0.995 C	20–250°C: 0.240 CO + 0.006 CO_2 250–450°C: 0.268 CO + 0.090 CO_2	175, 375, 500
0.05	0.819 CO + 0.100 CO_2 Σ = 0.920 C	20–270°C: 0.284 CO + 0.005 CO_2 270–450°C: 0.276 CO + 0.026 CO_2	225, 375, 500
0.11	0.871 CO + 0.129 CO_2 Σ = 1.00 C	20–280°C: 0.343 CO + 0.005 CO_2	250, 390, 500
0.30	0.923 CO + 0.117 CO_2 Σ = 1.040 C	20–250°C: 0.274 CO 250–450°C: 0.351 CO + 0.070 CO_2	125, 400, 500
1.1	1.147 CO + 0.004 CO_2 Σ = 1.151 C	20–210°C: 0.180 CO	120, 500

[a] The temperature range indicated in Fig. 5 with tic mark.

[b] The accumulated amount of gases evolved after temperature reached 500°C and was held for 30 min.

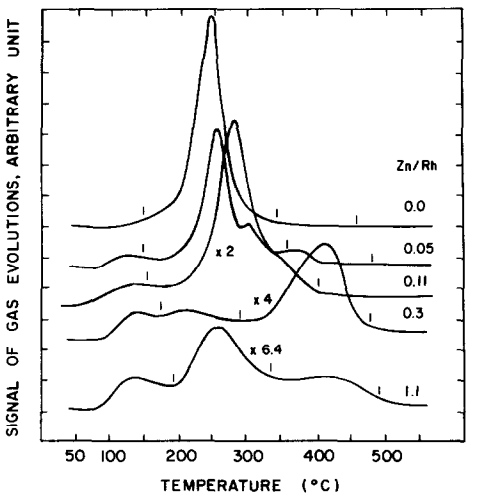

FIG. 6. Temperature-programmed desorption in hydrogen of CO chemisorbed at room temperature: carrier gas = 30 cm^3/min hydrogen, heating rate = 10°C/min.

with identifiable maxima at 175, 350, and 500°C. It is clear that the addition of Zn monotonically reduced the amount of CO desorbed below 400°C. The peak at 350°C shifted to 400°C as the Zn/Rh ratio increased from 0.0 to 0.3. For Zn/Rh = 1.1 this maximum disappears and only two peak maxima are observed. The total amount of desorbed gases was close to 1 C/Rh_s for each sample. The accumulated amount of CO_2 evolved was about the same for Zn/Rh in the range 0.0 to 0.3, but for Zn/Rh = 1.1 the amount of evolved CO_2 fell to almost zero.

The TPD scans into a H_2 flow are shown in Fig. 6 and Table 6. In the case of Rh/SiO_2, most of the chemisorbed CO was desorbed as CH_4; only a small fraction of unreacted CO desorbed around 125°C. With increasing Zn content the fraction of the adsorbate released as CH_4 decreased, and for Zn/Rh = 1.1, roughly 90% of the CO desorbed unreacted.

DISCUSSION

Coverage of Rh Surface by Zn

An important conclusion from the CO and H_2 chemisorption, XPES, and IR data is that the rhodium surface is partially covered with a zinc-containing overlayer. For example, the CO adsorption on the Zn/Rh = 0.3 sample amounts to only 45% of that

TABLE 6

Gas Evolution from TPD of Chemisorbed CO in H_2

Zn/Rh	Gas evolution in specified range[a] (per Rh_s)	Position of CH_4 peak (°C)	Total CH_4 (per Rh_s)
0.00	20–140°C: 0.013 CO + 0.007 CH_4 140–340°C: 0.027 CO + 1.029 CH_4 340–460°C: 0.000 CO or CH_4	240	1.036
0.05	20–140°C: 0.100 CO + 0.002 CH_4 140–360°C: 0.077 CO + 0.842 CH_4 360–480°C: 0.035 CH_4	252	0.879
0.11	20–150°C: 0.114 CO + 0.002 CH_4 150–400°C: 0.096 CO + 0.852 CH_4	285	0.854
0.30	20–170°C: 0.280 CO 170–290°C: 0.270 CO + 0.004 CH_4 290–470°C: 0.159 CO + 0.590 CH_4	420	0.594
1.1	20–190°C: 0.240 CO 190–330°C: 0.559 CO + 0.008 CH_4 330–485°C: 0.298 CO + 0.129 CH_4	435[b]	0.137

[a] The range is specified in Fig. 6 by the tic marks.
[b] CO makes a substantial contribution to this peak.

on Rh/SiO_2. From the TEM data it appears that no change in Rh particle size is induced by Zn. Once the Zn coverage of the surface Rh has reached a saturation level, further addition of Zn leads to Zn chloride or oxychloride particles located on the support surface. This can be derived from the XPS results in Table 3. While the overall Zn/Rh ratio is increased by a factor of 2.6 (from 0.3 to 1.1), the peak area ratio Zn/Rh increases by only 36%, but the Cl/Zn area ratio increases by a factor of 2.4. Apparently, the Zn chloride (or oxychloride) particles on the SiO_2 surface are able to retain much of their chlorine during the reduction treatment.

The Zn-containing adlayer on the rhodium particles suppresses the bridging mode of adsorbed CO more than the linear mode. With an overall Zn/Rh ratio of 0.3 the bridging CO is completely suppressed (Fig. 2B). A similar suppression of bridging CO was found for CO adsorbed on Pd when alloyed with Ag (*25*). Apparently some atoms of the overlayer block the ensembles of surface Rh atoms that are required for the bridging CO complex. If Zn is present in the form of cations, electroneutrality requires that an equivalent number of anions also be present, such as oxide ions. The detection of this overlayer is therefore reminiscent of effects observed with transition metals supported on partially reduced titanium dioxide, where it has been proven that the metal particles are partially covered or totally encapsulated by an overlayer of reduced titanium oxide (*26, 27*). It is known that ions adsorbed on metals prefer positions where they are in contact with several surface metal atoms (*28*); so it is plausible that both the zinc ions and the coadsorbed counterions will be located on such "Freundlich sites" on the Rh surface.

For Zn/Rh = 0.3 or 1.1 the number of chemisorbed CO molecules exceeds the number of adsorbed H atoms about twofold. Again, this can be rationalized in terms of the decreased size of the adsorbing Rh ensembles: H_2 is dissociative chemisorbed, while CO can be chemisorbed on a single Rh atom without dissociation. The dissociative chemisorption of H_2 will therefore be suppressed more than the CO adsorption, when site blocking by the Zn-containing overlayer is significant. Similarly, for Pt–Sn and Ru–Cu alloys, a larger than linear suppression of hydrogen chemisorption has been reported due to alloying with Cu, and the result was attributed to this "ensemble" effect (*29, 30*).

Before further discussing the effects of the zinc-containing overlayer on the Rh surface, it is important to decide which element of the overlayer is dominantly responsible for the observed effects. Kip *et al.* found that little Cl (0.1 mol% from XPS) was retained on Rh/SiO_2 after reduction of $RhCl_3/SiO_2$ at 350°C (*31*). Similarly, no XPS detectable Cl signal was found in the present study (Table 3) for Rh/SiO_2 prepared from $RhCl_3$, after reduction at 400°C. As shown above, the chlorine signal detected for samples with Zn/Rh = 0.3 and 1.1 is due to Zn chloride or oxychloride particles on the support, while for the low-Zn/Rh samples the Zn resides on the Rh surface, but the chlorine is removed either by reduction or by anion exchange with OH groups of desorbed water. A variety of metal chlorides, which have been added to Rh/SiO_2, display pronounced *metal-specific* promoter effects in the catalysis of CO hydrogenation and olefin hydroformylation (*4, 5, 8, 14*). Among these, zinc was found to increase hydroformylation activity significantly (*15*). In our opinion, these facts justify the view that zinc is the decisive species in the adlayer covering the Rh particles.

Effect of Promoter on Desorption Kinetics

It has been shown that hydrogen adsorbed on a Rh tip (*32*) or on some single-crystal faces of Rh (*33, 34*) desorbs in a single peak. However, adsorbed hydrogen desorbed in two peaks for Rh/SiO_2 (*35*) and three peaks for Rh/TiO_2 (*36*). The broad peaks in the hydrogen TPD found in the

present work indicate merged desorption peaks, that are typical of nonhomogeneous surfaces. The suppression by Zn of the hydrogen desorption band on the high-temperature side implies that the Zn promoter preferentially occupies strong chemisorption sites for hydrogen. Likewise, the multiple desorption peaks of CO in He reveal multiple adsorption sites. Figure 5 shows a decrease in the fraction of CO desorbed below 400°C and a slight upward shift in the high-temperature TPD peak. This could indicate some weak, but positive interaction between CO and coadsorbed Zn ions, similar to CO and K on Ni (*37*) and other transition metals.

The most prominent effect of Zn on desorption kinetics is, however, visible in the reductive desorption of CO in a flow of hydrogen. The results in Table 6 show that the formation of methane is strongly affected by the Zn-containing overlayer. The peak temperature for this reaction increases with increased Zn/Rh ratio and the fraction of adsorbed CO that is converted to methane rather than desorbed unreacted changes dramatically. Some 96% of the adsorbed CO leaves the surface as methane in the absence of the promoter, but for Zn/Rh = 1.1, this fraction dropped to roughly 10%. Methane formation on transition metal catalysts requires dissociative adsorption of CO (*14, 38–40*), so it appears safe to conclude that the presence of Zn strongly suppresses the dissociation of CO. Also, the results for CO desorption into a helium flow are consistent with this conclusion: the absence of CO_2 in the desorbate from the Zn/Rh = 1.1 sample shows that the Boudouard reaction, requiring CO dissociation, has been totally suppressed. Dissociative adsorption of hydrogen might also be impeded, but the consequences are less drastic because dissociation on a small number of exposed sites followed by surface migration of adsorbed H atoms will suffice to populate all other accessible sites.

Additional possible causes contributing to the drastic suppression of methane formation are the lower concentration of adsorbed hydrogen and the reduced mobility of the H atoms over the surface. However, if CO dissociation is a unidirectional process, as has often been assumed (*14*), the suppression of this dissociation becomes the single cause for the suppression of methane formation.

In previous work it appeared that manganese promotes the formation of higher oxygenates in the hydrogenation of CO over Rh/SiO_2, and the data indicated that this promoter enhances the TOF for CO dissociation. The Zn promoter which increases the formation of methanol, not higher oxygenates, appears to act differently, and as the above data show, this promoter strongly suppresses the dissociation of CO. This shows that different explanations are required for the effects of different promoters.

IR Evidence for the Nature of Adsorbed CO

To gain more detailed information on the mode of bonding of CO to zinc-promoted rhodium, infrared spectra were collected as a function of added Zn. In the absence of Zn the spectrum of CO adsorbed on Rh/SiO_2 contains a prominent band at 2054 cm^{-1} associated with linear CO, which is not significantly influenced by added zinc. The broadband with indistinct maxima around 1912 and 1855 cm^{-1}, which is characteristic of bridging CO, disappears as zinc is added to the system and a shoulder around 1960 cm^{-1} grows in. Thus, the predominant influence of zinc is to decrease in the intensity of the bridging CO bands, which was discussed above in terms of site blocking. The 1960 cm^{-1} feature appears to be too high to be assigned to bridging CO.

One of the mechanisms proposed for oxygenate formation is based on the presence of Rh(I), which appears to be induced by electropositive ions (*2, 41*) We therefore inspected the IR spectra for evidence of Rh(I). The diagnostic bands are the linear CO stretch around 2100 for a surface

$Rh^{I}CO$ and the presence of bands at 2030 and 2090 cm^{-1} for $Rh^{I}(CO)_2$ (*42*). The spectrum (Fig. 2) indicates that neither is present in significant amount. There is no hint of a 2100 cm^{-1} band. The possibility of a band at 2030 cm^{-1} cannot be assessed because this region is obscured by the strong band at ca. 2054 cm^{-1}. The other component of the *gem*-dicarbonyl stretch should be observable at 2090 cm^{-1}. The spectra show a very weak feature around this frequency for Rh/SiO_2 in the absence of zinc. As the zinc concentration in the sample is increased this weak 2090 cm^{-1} feature appears to decrease and it is not observable when Zn:Rh is 1.1:1. Thus the IR data give no indication of the production of Rh(I) carbonyl species in the presence of zinc.

The weak bands in the vicinity of 1600 cm^{-1} also are potentially revealing. This region of the spectrum is notorious for interfering bands, but experiments with ^{13}CO and CO_2, displayed in Fig. 3 and described under Results, indicate that a major part of the ca. 1597 cm^{-1} band is derived from CO and not surface water, carbonate, or bicarbonate. However, these results indicate that, contrary to our previous report (*20*), the band at 1620 cm^{-1} arises primarily from the support.

There are three likely remaining assignments for the 1597 cm^{-1} band, surface formyl, formate, or tilted CO. Table 7 presents some of previous assignments for these types of species. In general the assignments for organometallics are more certain than those for surface species, but the organometallics are not perfect models. The data in Table 3 lead to the conclusion that the 1597 cm^{-1} band observed for CO on our $RhZn/SiO_2$ samples, will fit all three possibilities.

Sodium formate is known to have an additional band at 1366 and 1377 cm^{-1} (*43*) and a similar feature has been reported for surface formate (Table 3). A band is observed at 1380 cm^{-1} for the $RhZn/SiO_2$ treated with normal isotopic CO and 1354 cm^{-1} when ^{13}CO was employed (Fig. 3). This observation is consistent with the presence of formate, but the presence and position of these bands are subject to uncertainty because they appear after subtraction of the rapidly rising SiO_2 background. An independent check on the presence of formate is in principle possible from CO_2 determined in the TPD experiment; however, IR indicates too little formate would be present to detect by this method.

TABLE 7

Assignments for Some Surface and Organometallic Formates, Formyls, and C- and O-bonded Carbonyls

Band (cm^{-1})	Species[a]	System	Reference
1567, 1366	Formate	Inorganic	(*43*)
ca. 1600	Formate	$HCOH-Rh/Al_2O_3$	(*44*)
1595, 1380	Formate	$CO + H_2$ on Rh/Al_2O_3 or Rh/MgO	(*45*)
1520	Formyl	$CO + H_2$ on ZnO	(*46*)
1530–1630	Formyl	Organometallic	(*47*)
1545–1750	—CO—	Organometallic	(*48*)
1438–1761	>CO—	Organometallic	(*48*)
1580	—CO—	Cu/ZnO	(*34*)

[a] Assignments are from the references cited.

CONCLUSION

The XPES, chemisorption, and TPD data presented here demonstrate that zinc (oxide) forms a partial overlayer on rhodium supported on SiO_2. These observations are in harmony with a model that we previously proposed for the reduction of methane formation by adding zinc to Rh/SiO_2. In that model it was proposed that the zinc blocks sites on which CO cleavage occurs. The IR data indicate that the zinc reduces the proportion of bridging CO. The IR data, however, are inconclusive on the issue of why zinc promotes the formation of oxygenates. In one model, oxygenate formation is attributed to the presence of Rh(I) species, but IR data indicated that Rh(I) coordinated to CO was not detected upon addition of zinc to the surface. In another model, C- and O-bonded CO is invoked to explain enhanced CO migratory insertion, which is

part of the proposed route to oxygenates. A ca. 1597 cm^{-1} band in the IR spectrum of CO adsorbed on $ZnRh/SiO_2$ is attributed to one of three possibilities: formyl, formate, or a C- and O-bonded CO. The IR data do not permit us to distinguish between these possibilities.

ACKNOWLEDGMENTS

This research was sponsored by the DOE through Grant DE-FG02-85ER45220. We also thank Johnson Mathey for the loan of the rhodium metal used in this research.

REFERENCES

1. Rabo, J. A., Risch, A. R., and Poutsma, M. L., *J. Catal.* **53,** 295 (1978).
2. (*a*) Wilson, T. P., Kasai, P. H., and Ellgen, P. C., *J. Catal.* **69,** 193 (1981). (*b*) Ellgen, P. C., Bartley, W. J., Bhasin, M. M., and Wilson, T. P., *ACS Adv. Chem. Ser.* **178,** 147 (1979).
3. Ichikawa, M. (*a*) *Bull. Chem. Soc. Japan* **51**(8), 2268 (1978). (*b*) *Bull. Chem. Soc. Japan* **51**(8), 2273 (1978). (*c*) *Chemtech*, 674 (1982).
4. (*a*) Ichikawa, M., Fukushima, T., and Shikakura, K., *in* "Proceedings, International Congress on Catalysis, 8th," Vol. II, p. 69 (1984). (*b*) Fukushima, T., Arakawa, H., and Ichikawa, M., *J. Phys. Chem.* **89,** 4440 (1985). (*c*) ibid., *J. Chem. Soc. Chem. Commun.*, 729 (1985). (*d*) Ichikawa, M., and Fukushima, T., *J. Chem. Soc. Chem. Commun.*, 321 (1985).
5. (*a*) Kikuzono, Y., Kagami, S., Naito, S., Onishi, T., and Tamaru, K., *Faraday Discuss. Chem. Soc.* **72,** 135 (1981). (*b*) Naito, S., Yoshioka, H., Orita, H., and Tamaru, K., *in* "Proceedings, International Congress on Catalysis, 8th," Vol. III, p. 207 (1984).
6. (*a*) Ryndin, Yu. A., Hicks, R. F., and Bell, A. T., *J. Catal.* **70,** 287 (1981). (*b*) Hicks, R. F., and Bell, A. T., *J. Catal.* **90,** 205 (1984). (*c*) ibid., *J. Catal.* **91,** 104 (1985).
7. Poels, E. K., Van Broekhoven, E. H., Van Barneveld, W. A. A., and Ponec, V., *React. Kinet. Catal. Lett.* **18,** 223 (1981).
8. (*a*) Poels, E. K., Koolstra, R., Geus, J. W., and Ponec, V., *Stud. Surf. Sci. Catal.* **11,** 233 (1982). (*b*) Driessen, J. M., Poels, E. K., Hinderman, J. P., and Ponec, V., *J. Catal.* **82,** 26 (1983).
9. (*a*) Sudhakar, C., and Vannice, M. A., *J. Catal.* **95,** 227 (1985). (*b*) Vannice, M. A., Sudhakar, C., and Freeman, M., *J. Catal.* **108,** 97 (1987).
10. (*a*) Orita, H., Naito, S., and Tamaru, K., *J. Chem. Soc. Chem. Commun.*, 150 (1984). (*b*) ibid., *J. Catal.* **90,** 183 (1984).
11. Van den Berg, F. G. A., Glezer, J. H. E., and Sachtler, W. M. H., *J. Catal.* **93,** 340 (1985).
12. (*a*) Favre, T. L. F., Van der Lee, G., and Ponec, V., *J. Chem. Soc. Chem. Commun.*, 230 (1985). (*b*) Kowalski, J., Van der Lee, G., and Ponec, V., *Appl. Catal.* **19,** 423 (1985).
13. Kip, B. J., Hermans, E. G. F., and Prins, R., *Appl. Catal.* **35,** 109, 141 (1987).
14. (*a*) Sachtler, W. M. H., *in* "Proceedings, International Congress on Catalysis, 8th," Vol. I, p. 151 (1984). (*b*) ibid., *Actas X Simp. Iberoam. Catal.* 1327 (1986). (*c*) Sachtler, W. M. H., and Ichikawa, M., *J. Phys. Chem.* **90,** 4752 (1986).
15. (*a*) Sachtler, W. M. H., Shriver, D. F., Hollenberg, W. B., and Lang, A. F., *J. Catal.* **93,** 429 (1985). (*b*) Sachtler, W. M. H., Shriver, D. F., and Ichikawa, M., *J. Catal.* **99,** 513 (1986).
16. Van der Lee, G., and Ponec, V., *J. Catal.* **99,** 511 (1986).
17. (*a*) Shriver, D. F., *ACS Symp. Ser.* **152,** 1 (1981). (*b*) Horwitz, C. P., and Shriver, D. F., *Adv. Organometall. Chem.* **23,** 219 (1984). (*c*) Tessier-Youngs, C., Correa, F., Pioch. D., Burwell, R. L., Jr., and Shriver, D. F., *Organometallics* **2**(7), 898 (1983).
18. (*a*) Santos, J., Phillips, J., and Dumesic, J. A., *J. Catal.* **81,** 147 (1983). (*b*) Vannice, M. A., Twu, C. C., and Moon, S. H., *J. Catal.* **79,** 70 (1983). (*c*) Correa, F., Nakamura, R., Stimson, R. E., Burwell, R. L., Jr., and Shriver, D. F., *J. Amer. Chem. Soc.* **102,** 5112 (1980). (*d*) Richmond, T. G., Basolo, F., and Shriver, D. F., *Inorg. Chem.* **21,** 1272 (1982).
19. Butts, S. B., Holt, E. M., Strauss, S. H., Alcock, N. W., Stimson, R. E., and Sriver, D. F., *J. Amer. Chem. Soc.* **101,** 5864 (1979).
20. Ichikawa, M., Lang, A. J., Shriver, D. F., and Sachtler, W. M. H., *J. Amer. Chem. Soc.* **107,** 7216 (1985).
21. (*a*) Yang, A. C., and Garland, C. W., *J. Phys. Chem.* **61,** 1504 (1957). (*b*) Garland, C. W., Lord, R. C., and Troiano, P. F., *J. Phys. Chem.* **69,** 1188 (1965).
22. Guerra, C. R., and Schulman, J. H., *Surf. Sci.* **7,** 229 (1967).
23. Yao, H. C., and Rothschild, W. G., *J. Chem. Phys.* **68**(11), 4774 (1978).
24. (*a*) Eischens, R. P., Francis, S. A., and Pliskin, W. A., *J. Phys. Chem.* **60,** 194 (1956). (*b*) Eischens, R. P., *Acc. Chem. Res.* **5,** 74 (1972).
25. (*a*) Soma-Noto, Y. and Sachtler, W. M. H., *J. Catal.* **32,** 315 (1974). (*b*) ibid., *J. Catal.* **34,** 162 (1974). (*c*) Primet, M., Matthieu, M., and Sachtler, W. M. H., *J. Catal.* **44,** 324 (1976).
26. Sadeghi, H. R., and Henrich, V. E., *J. Catal.* **87,** 279 (1984).
27. Takatani, S., and Chung, Y.-W., *J. Catal.* **90,** 75 (1984).
28. Sachtler, W. M. H., *Ultramicroscopy* **20,** 135 (1986).

29. Verbeek, H., and Sachtler, W. M. H., *J. Catal.* **42,** 257 (1976).
30. (*a*) Shimizu, H., Christmann, K., and Ertl, G., *J. Catal.* **61,** 412 (1980). (*b*) Vickerman, J. C., and Christman, K., *Surf. Sci.* **120,** 1 (1982).
31. Kip, B. J., Dirne, F. W. A., Van Grondelle, J., and Prins, R., *Prepr. Div. Petrol. Chem. ACS* **31** (1), 163 (1986).
32. Gorodetskii, V. V., Nieuwenhuys, B. E., Sachtler, W. M. H., and Boreskov, G. K., *Surf. Sci.* **108,** 225 (1981).
33. (*a*) Castner, D. G., Sexton, B. A., and Somorjai, G. A., *Surf. Sci.* **71,** 519 (1978). (*b*) Castner, D. G., and Somorjai, G. A., *Surf. Sci.* **83,** 60 (1979).
34. Boccuzzi, F., and Chiorino, A., *J. Chem. Soc. Chem. Commun.*, 1012 (1985).
35. Chin, A. A., and Bell, A. T., *J. Phys. Chem.* **87,** 3482 (1983).
36. Apple, T. M., Gajardo, P., and Dybowski, C., *J. Catal.* **68,** 103 (1981).
37. Urane, K. J., Ng, L., and Yates, J. T., Jr., *Prepr. Div. Petrol. Chem. ACS* **31**(1), 295 (1986).
38. Araki, M., and Ponec, V., *J. Catal.* **44,** 430 (1976).
39. Biloen, P., Helle, J. N., and Sachtler, W. M. H., *J. Catal.* **58,** 95 (1979).
40. Low, G. G., and Bell, A. T., *J. Catal.* **57,** 397 (1979).
41. Watson, P. R., and Somorjai, G. A., *J. Catal.* **44,** 430 (1976).
42. Rice, C. A., Worley, S. D., Curtis, C. W., Guin, J. A., and Tarrer, A. R., *J. Chem. Phys.* **74**(11), 6487 (1981).
43. Nakamoto, K., "Infrared and Raman Spectra of Inorganic and Coordination Compounds," 4th ed., p. 232. Wiley, New York, 1986.
44. Yates, J. T., Jr., and Cavanagh, R. R., *J. Catal.* **74,** 97 (1982).
45. Solymosi, F., Tombacz, I., and Kocsis, M., *J. Catal.* **95,** 41 (1985).
46. Lavalley, J. C., Saussey, J., and Rais, T., *J. Mol. Catal.* **17,** 289 (1982); Saussey, J., Lavalley, J. C., Lamotte, J., and Rais, T., *J. Chem. Soc. Chem. Commun.*, 278 (1982).
47. Gladysz, J. A., *Adv. Organometall. Chem.* **20,** 1 (1982).
48. Horwitz, C. P., and Shriver, D. F., *Adv. Organometall. Chem.* **23,** 219 (1984).